IEEE Access
Multidisciplinary | Rapid Review | Open Access Journal

Received April 20, 2016, accepted May 16, 2016, date of publication July 11, 2016, date of current version August 15, 2016.

Digital Object Identifier 10.1109/ACCESS.2016.2584980

Exploiting Site-Specific Propagation Characteristics in Directional Search at 28 GHz

JUAN C. AVILES[1,2], (Member, IEEE), AND AMMAR KOUKI[2], (Senior Member, IEEE)
[1]Faculty of Electrical and Computer Engineering, Escuela Superior Politécnica del Litoral, Km 30.5 Via Perimetral, P.O.Box. 09-01-5863, Guayaquil, Ecuador
[2]Electrical Engineering Department, École de Technologie Supérieure, Montreal, QC H3C 1K3, Canada

Corresponding author: J. C. Aviles (javiles@espol.edu.ec)

This work was supported in part by the Escuela Superior Politécnica del Litoral, Guayaquil, Ecuador, and in part by the École de Technologie Supérieure, Montreal, Canada.

ABSTRACT Simulation data from a ray-tracing tool applied in specific urban environments in the 28-GHz band suggest that the utilization of arbitrary base station (BS) angles in a directional search procedure may not be of maximum benefit for users located in non-line-of-sight positions, because certain angles restrict the radio frequency illumination to a lower maximum power than from others. An appropriate selection of BS angles offers a potential power level benefit of greater than 2 dB in a defined number of consecutive measurements; however, this performance improvement appears to be conditioned by the severity of the existing street canyon propagation and the probability of the angle used. A simple ray tracing method is proposed to approximately identify the most effective BS angles that avoid power emissions in directions largely blocked by nearby buildings. The results indicate that prior site-specific information may be helpful, particularly for systems using analog beamforming.

INDEX TERMS Angle of arrival, base station, beam direction, millimeter wave, non-line-of-sight, radio frequency, ray tracing, user equipment.

I. INTRODUCTION

With the increasing adoption of mobile devices (e.g., smartphones), demand for cellular wireless capacity is projected to grow at a rate that would not be supported by current networks [1]. Therefore, there has been increasing interest in cellular systems based on the so-called millimeter-wave (mmW) bands (30-300 GHz) because such systems provide the possibility of a larger spectrum allocation than that obtained for cellular systems below 3 GHz [2]. Specifically, the 28-38 GHz band is currently considered to have strong potential to provide 5th-generation cellular services. In this regard, measurements in New York City indicate that modern building materials are good reflectors, which facilitates outdoor non-line-of-sight (NLOS) links and radiofrequency (RF) power contention within buildings [3]. Moreover, there are a large number of distinguishable propagation paths at any receiver position in both line-of-sight (LOS) and NLOS locations, with an average of 2.5 signal lobes (each with an average total and root mean square (RMS) angle spread of 40.3° and 7.8°, respectively), allowing feasible links with the help of high-gain steerable antennas in cell sizes of approximately 200 m [4], [5]. Significant NLOS outdoor street-level coverage was possible within this range even in urban canyon environments [6]. Measurements at the University of Texas showed that elevated 38 GHz transmitters using beam steering may require up to ±30° off boresight in azimuth to cover nearly all possible NLOS links within the study area, and for cases in which the LOS direction is blocked, there is a reflection, scattered or diffraction path that permits the user equipment (UE) to receive sufficient power [7], [8].

Due to the large propagation path loss, a communication link must be "found" through the application of high-gain directional antennas that can be implemented with beamforming techniques. However, new procedures must be designed to utilize these techniques because their application is different from those in cellular systems operating at microwave frequencies, where the beamforming typically takes effect after the user obtains an access connection [9], [10] and not for the access itself. Under random access, it is difficult to utilize the beamforming gain due to insufficient knowledge of the optimal beam combinations [11], particularly for NLOS environments. Digital beamforming would offer more flexibility in directional cell search methods in which the base station (BS) periodically transmits a synchronization signal in random directions [12]; nevertheless, the number of RF front ends required becomes

costly, and it would not be practical for the UE. In contrast, analog beamforming, although limited due to its inherent 'one-look direction', offers advantages because it uses a single RF front-end with reduced cost, complexity and power consumption. Despite that shortcoming, which poses significant challenges in a BS-UE initial connection, there is increasing interest in analog beamforming in mmW wireless systems used alone or in combination with digital precoding in a hybrid solution [13], [14].

Evidently, much research effort for directional search in mmW bands is directed to seek the most suitable propagation paths. This task is complex due to the presence of blocking (i.e., the probability that the mmW signal is completely blocked) [15]. RF illumination using some BS-UE beam directions may be sufficiently blocked by nearby buildings that their application could be considered an inefficient use of power. This inefficient use generates a potential lack of an appropriate power level at an NLOS position, even at short distances from a BS, which prevents a guaranteed feedback from the UE. In contrast, there is a high probability that the best antenna orientations are only in the direction of the streets (street canyon propagation), which does not favor the general use of a complete set of equally spaced BS angles for transmission of the synchronization signals.

One line of research that has not been fully explored is based on the concept of utilizing the knowledge of the propagation characteristics of the service area. In [16], indoor simulations (60 GHz) suggested that prioritizing the search in certain directions determined from operational statistics speeds up the link configuration compared to a traditional exhaustive search. Cognition of the site-specific propagation characteristics can be exploited in the initial stage of the NLOS BS-UE connection procedure in the 28-38 GHz band, particularly for systems using analog beamforming.

Because the propagation information is site specific, we first propose a simplified ray-tracing (RT) procedure to identify the most effective BS and UE angles in terms of the maximum received power at any position of the user. Second, the application of the reduced set of identified BS angles is demonstrated to have the potential to increase the average signal-to-noise ratio (SNR) in a defined number of power measurements compared to that obtained using arbitrary angles. Moreover, given that the same best BS and UE discrete angles may be repeated individually or together at many different geographical positions, it is also shown that their percentage distribution at the NLOS positions can also be exploited for further improvement. The performance benefit using this reduced set of angles is determined in two scenarios with different street canyon propagation characteristics. For this task, we contrast the improvement in the SNR when both the BS and UE change their main beam orientations randomly and the difference in the number of angles switches used in a specific beam alignment method.

Potential advantages can be expected for cases such as those in which the BS simultaneously transmits in various directions using different pilot carrier frequencies [10], broadcasts synchronization signals periodically using a random switching of the beamforming vector angles [11], [12], exploits the knowledge of the best BS angles to avoid blocking in a channel estimation (MIMO) using hybrid beamforming [14] or uses the UE position and/or its associated context-based information for beamforming [17].

The remainder of the paper is organized as follows. Section II describes the system model and simulation methodology. An RT method for an approximate identification of the optimal angle ranges for the BS RF illumination is proposed in section III. Section IV presents applications of the selected angles. Finally, concluding remarks are provided in section V.

II. SYSTEM MODEL AND SIMULATION METHODOLOGY

A. SYSTEM MODEL

Consider a time division duplex (TDD) cellular system sector with dimensions of $60° \times 200$ m located in a specific urban environment where the BS and UE are equipped with directional antennas and apply discrete angles taken from well-defined sets. The UE is located at a NLOS position. The BS illuminates (downlink) the service area, whereas the UE measures the received power when both are randomly switching their antenna beams L times within a time period T. The UE determines the maximum received power at the end of each period.

To gain insight into the benefit of applying selected BS angles for RF illumination in a random access procedure, we first consider a simplified one-dimensional (1-D) scheme in which the UE receives only one multipath component with an angle of arrival (AoA) $\theta_{UEalign}$. Given that each BS angle θ_{iBS} renders a different RF spatial coverage, the UE reads a maximum power level $\tilde{A}_i$ (Fig. 1) when its antenna's main beam is aligned with respect to $\theta_{UEalign}$ (Fig. 2). We assume the BS uses $\theta_{iBS} \varepsilon \{\theta_{1BS}, \theta_{2BS}, .., \theta_{NBS}\}$, with $p_{\theta_{iBS}} = \text{Prob}(\theta_{iBS})$, and for each θ_{iBS} it is associated a maximum power level $\tilde{A}_i \varepsilon \left\{\tilde{A}_1, \tilde{A}_2, \ldots, \tilde{A}_N\right\}$, where $p_{\tilde{A}_i} = \text{Prob}(\tilde{A}_i) = p_{\theta_{iBS}}$ and $\tilde{A}_1 < \tilde{A}_2 < .... < \tilde{A}_N$.

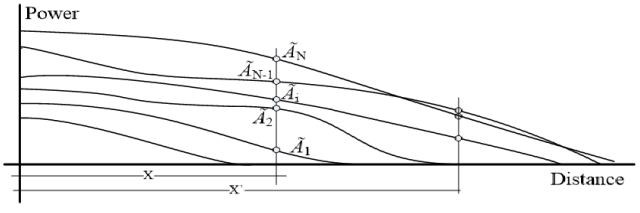

FIGURE 1. Illustration of 1-D maximum RF coverage for different BS angles.

For any UE angle, the received power is $Z = \tilde{A} g_u(\theta^{\Delta})$, where g_u is the gain of the UE antenna assumed to have the pattern in Fig. 3 [18] and Equation (1). $\theta^{\Delta} = (\theta_{UEalign} - \theta_{UE})$ is the difference in the UE azimuth angles between the UE antenna direction aligned with the arriving multipath component and an arbitrary orientation. The values of θ^{Δ} follow a

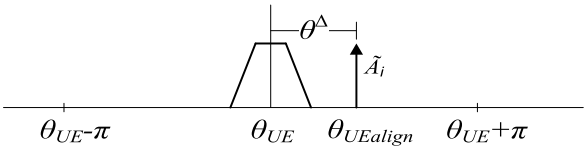

FIGURE 2. One multipath component arriving at the UE.

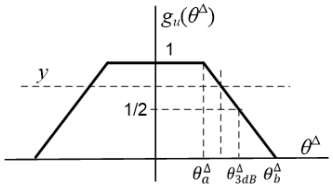

FIGURE 3. UE antenna gain.

uniform distribution, i.e., $\theta^{\Delta} \sim \mathrm{U}(-\pi,\pi]$.

$$y = g_u(\theta^{\Delta}) = \begin{cases} 1 & |\theta^{\Delta}| \le \theta_a^{\Delta} \\ \left|1 - \dfrac{|\theta^{\Delta}| - \theta_a^{\Delta}}{2\left(\theta_{3dB}^{\Delta} - \theta_a^{\Delta}\right)}\right| & \theta_a^{\Delta} < |\theta^{\Delta}| \le \theta_b^{\Delta} \\ 0 & \theta_b^{\Delta} < |\theta^{\Delta}| \le \pi \end{cases} \tag{1}$$

The cumulative distribution function (*cdf*) of Z in the range $\tilde{A}_{j-1} \le z < \tilde{A}_j; j = 1, 2, \ldots, N$, for any antenna orientation can be calculated [19] as follows (Appendix A):

$$F_Z(z) = \left(1 - \frac{\theta_b^{\Delta}}{\pi}\right) + \left(\frac{\theta_b^{\Delta}}{\pi}\right) \sum_{i=1}^{j-1} p_{\tilde{A}_i} + \left(\frac{\theta_b^{\Delta} - \theta_a^{\Delta}}{\pi}\right) z \left[\sum_{i=j}^{N} \frac{p_{\tilde{A}_i}}{\tilde{A}_i}\right] \tag{2}$$

After L measurements Z_l (considered independent random variables), the maximum UE power read and its *cdf* can be written as follows [19]:

$$\hat{Z} = \max\left[Z_1 \quad Z_2 \ldots\ldots \quad Z_L\right] \tag{3}$$

$$F_{\hat{Z}}(\hat{z}) = F_{Z_1}(\hat{z}) F_{Z_2}(\hat{z}) \ldots F_{Z_l}(\hat{z}) \ldots F_{Z_L}(\hat{z}) \tag{4}$$

where $F_{Z_l}(\hat{z})$ (l=1,2,..,L) is given by (2). Fig. 4 shows plots of three individual $F_{Z_l}(\hat{z})$ for the particular cases of a) arbitrary $\tilde{A}_i$ and $p_{\theta_{iBS}} = p_{\tilde{A}_i} = P_i$ values ($\tilde{A}_{\mathrm{ia}}$, $\mathrm{P_{ia}}$ - black o) considered as a reference, b) the same P_i values but increased $\tilde{A}_i$ values ($\tilde{A}_{\mathrm{ib}}$, $\mathrm{P_{ia}}$ - black square) and c) the same $\tilde{A}_i$ values but with an increased probability for the higher $\tilde{A}_i$ values ($\tilde{A}_{\mathrm{ia}}$, $\mathrm{P_{ic}}$ - black Δ). We assumed that $\theta_{3dB}^{\Delta} = 6.5°$, $\theta_a^{\Delta} = 3°$, $\theta_b^{\Delta} = 10°$, $L = 3$, and $N = 8$ for the simulation.

For an arbitrary level *arlv*, $F_{Z_l}(arlv)$ calculated with the parameters of case 'b' is lower than that of case 'a' because the third term of (2) decreases with larger $\tilde{A}_i$ values. Similarly, F_{Z_l} (*arlv*) evaluated with the parameters

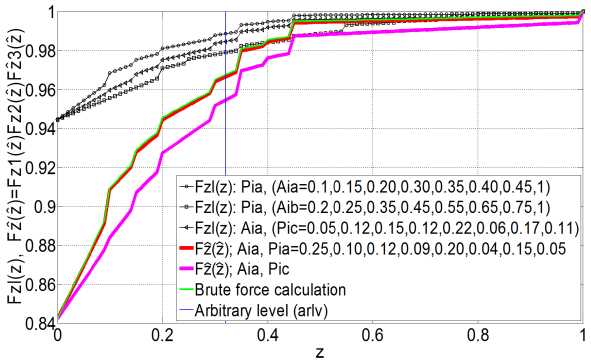

FIGURE 4. *cdf* of Z_l and $\hat{Z} = \max[Z_1 Z_2 \ldots\ldots Z_L]$, $L = 3$, $N = 8$.

of case 'c'[1] is lower than that of case 'a' because the decrease in value of the second term in (2) is greater than the increase of the third term. Such results are enhanced for $\hat{Z} = \max(Z_1, Z_2, \ldots, Z_L)$ with $F_{\hat{Z}}(\hat{z}) = \prod_{l=1}^{L} F_{Z_l}(\hat{z})$ in L UE power readings. The red and magenta curves in Fig. 4 show that $F_{\hat{Z}}(\hat{z}) \le F_{Z_l}(\hat{z})$ and $F_{\hat{Z}}(\hat{z})$ calculated with the parameters of case 'c' is lower than that of case 'a'. A decreased $F_{\hat{Z}}(\hat{z})$ implies a better system performance. In order to validate equations (2) and (4), we applied a brute force procedure (green dotted line) to determine the values of $F_{\hat{Z}}(\hat{z})$, that is, we generated θ^{Δ} and $\tilde{A}_i$ according to a uniform distribution and the probabilities of case 'a', respectively, calculated the antenna gain g_u using (1) and the power level as $Z_i = \tilde{A}_i g_u$. This process was repeated $L = 3$ times in each of the 35,000 iterations.

Given L and $N\tilde{A}_i$ values (or equivalently $N\theta_{iBS}$ angles), we can calculate $F_{\hat{Z}}(\hat{z}) = F_{\hat{Z}_2}(\hat{z})$ for any combination $C(N, n_o) = \binom{N}{n_o} = \frac{N!}{n_o!(N-n_o)!}$ of $n_o\tilde{A}_i$ values with $p_{\tilde{A}_i} = 0$ and the remaining $(N - n_o)\tilde{A}_i$ values with $p_{\tilde{A}_i} = 1/(N - n_o)$, and $F_{\hat{Z}_1}(\hat{z})$ with $p_{\tilde{A}_i} = 1/N$ assigned to all $N\tilde{A}_i$ values. Using (2) and (4), it is easy to show mathematically that $F_{\hat{Z}_2}(\hat{z})$ decreases relative to $F_{\hat{Z}_1}(\hat{z})$ if the zero probability was applied to the n_o lowest values of $\tilde{A}_i$. Moreover, the application of zero probability to the $(n_o + 1)$ lowest values of $\tilde{A}_i$ and equally increasing the probability $(1/(N - n_o - 1))$ to the remaining values, decreases $F_{\hat{Z}_2}(\hat{z})$ even more. For other cases in the set of $C(N, n_o)$ combinations, we used a simulation to assess them. Note that the application of $p_{\theta_{iBS}} = p_{\tilde{A}_i} = 0$ to a particular BS angle (discarded) results in a null contribution of its corresponding power level $\tilde{A}_i$ to $F_{Z_l}(z)$ in (2) because that angle is not used and that for any $C(N, n_o)$ in which $F_{\hat{Z}_2}(\hat{z}) \le F_{\hat{Z}_1}(\hat{z})$,

[1]This scheme also increases the total power $\check{Z} = \sum_{i=1}^{L} Z_i$ measured by the UE in L time slots, which in turn improves the cell detection when it is applied in a Generalized Likelihood Radio Test for cell search in systems using analog beamforming [12].

the UE has an increased probability to receive a higher power level in L power measurements using a reduced set of $(N - n_o)$ BS angles compared to that using the full set of N BS angles.

TABLE 1. Percentage of combinations in which $F_{\hat{Z}_1}(\hat{z}) - F_{\hat{Z}_2}(\hat{z}) \geq 0$.

C(N,n_o) in which $(p_{\tilde{A}_{i1}},.,p_{\tilde{A}_{ik}})\neq 0$ and there are n_o values of $(p_{\tilde{A}_i}=0)$ in the remaining (N-k) $\tilde{A}_i$ values.	$F_{\hat{Z}_1}(\hat{z}) - F_{\hat{Z}_2}(\hat{z}) \geq 0$			
	n_o=5	n_o=7	n_o=9	n_o=11
$(p_{\tilde{A}_{20}})\neq 0$	43.0	43.4	40.5	53.6
$(p_{\tilde{A}_{19}},p_{\tilde{A}_{20}})\neq 0$	58.4	68.7	76.9	86.3
$(p_{\tilde{A}_1},p_{\tilde{A}_2},p_{\tilde{A}_{19}},p_{\tilde{A}_{20}})\neq 0$	52.1	58.9	66.8	77.1
$(p_{\tilde{A}_1},p_{\tilde{A}_2},p_{\tilde{A}_{15}},p_{\tilde{A}_{19}},p_{\tilde{A}_{20}})\neq 0$	59.3	66.2	81.5	84.6
$(p_{\tilde{A}_1},p_{\tilde{A}_2},p_{\tilde{A}_5},p_{\tilde{A}_{19}},p_{\tilde{A}_{20}})\neq 0$	48.4	52.7	59.8	69.7

Table 1 shows the statistics of $\Delta F_{\hat{Z}}(\hat{z}) = F_{\hat{Z}_1}(\hat{z}) - F_{\hat{Z}_2}(\hat{z}) \geq 0$, obtained by using the general parameters $\theta_{3dB}^{\Delta} = 6.5°$, $\theta_a^{\Delta} = 3°$, $\theta_b^{\Delta} = 10°$, $N = 20$, $L = 50$ and a set $\mathcal{A}$ of realistic received power values[2] (normalized to 100 and sorted in ascending order). Four different cases (n_o = 5,7,9,11; $C(N, n_o)$ = 15504, 77520, 167960, 167960) were analyzed. In particular, $F_{\hat{Z}_1}(\hat{z})$ was calculated with $p_{\tilde{A}_i} = 1/20$ ($i = 1, 2, \ldots, 20$) whereas $F_{\hat{Z}_2}(\hat{z})$ was evaluated for particular groups of combinations in which k specific $\tilde{A}_i$ values were fixed with a probability different from zero. $\hat{Z}$ was allowed to take values in [0:0.01:100]. For any combination, the statistics of $\Delta F_{\hat{Z}}(\hat{z}) \geq 0$ were increased only in the event of a condition of compliance in at least 99.5% of its 10,001 values.

Table 1 indicates that there is an opportunity to decrease $F_{\hat{Z}_2}(\hat{z})$ in more than 50% of the combinations for those cases in which the BS angles associated with the largest $\tilde{A}_i$ values are not discarded. For a given n_o, the percentages increase as a greater number of the highest $\tilde{A}_i$ are considered (e.g., rows 1 vs. 2). Those combinations are not the only possibilities. There are cases where $F_{\hat{Z}_2}(\hat{z})$ decreases (>50%) if the BS angles linked to the maximum and minimum power values were taken into account (e.g., row 3). The typical large difference between the minimum and maximum $\tilde{A}_i$ values (>40dB) facilitates these results. Similarly, Table 1 shows that there cases in which the percentages of $\Delta F_{\hat{Z}}(\hat{z}) \geq 0$ increase with n_o as higher $\tilde{A}_i$ values are considered (e.g., rows 4 vs. 5).

Note that each row in Table 1 has a different maximum number of combinations (e.g., 48,620 for row 2; 11,440 for row 3). The percentage for each case is calculated using the fraction of those combinations in which $\Delta F_{\hat{Z}}(\hat{z}) \geq 0$ (e.g., 37,372 for row 2 and $n_o = 9$ (76.9%)).

[2] $\mathcal{A}$ = {[1.63305e-5, 2.00909e-5, 2.22331e-5, 2.96483e-5, 4.13048e-5, 5.17607e-5, 6.26614e-5, 1.24451e-4, 1.85353e-4, 5.82103e-4, 6.88652e-5, 1.28233e-3, 3.98107e-3, 6.83912e-3, 1.47571e-2, 3.23594e-2, 7.88860e-2, 1.74985e-1, 5.66239e-1, 1.00000]∗100}

Given that there is a high probability of blocking in urban environments, it is not difficult to find a group of n_o angles that do not help the BS deliver the maximum possible power level at any location in the service area. Setting a zero probability to the elements of that group and an increased probability value $(1/(N - n_o))$ to the remaining BS angles can improve the system performance. Specifically, if any of the $(N - n_o)$ BS angles was associated with the maximum possible received power level at an arbitrary position, that maximum level (i.e., an equivalent to $\tilde{A}_{20}$) would be included in (2). Because some of the other $(N - n_o - 1)$ angles also facilitate the delivery of the highest power levels at the position considered, the combined effect of the application of the best angles and the avoidance of those that do not help the BS deliver a maximum power level can generate the condition $\Delta F_{\hat{Z}}(\hat{z}) \geq 0$ for many locations of the service area.

Note that the exclusion of n_o BS angles has a different impact at each position of the user because those angles are not associated exclusively with the lowest power levels everywhere. Considering that the $\tilde{A}_i$values can be sorted in ascending order, two different geographical positions may have individual ordered sets of $N\tilde{A}_i$ values linked to different distributions of N BS angles (e.g., $\{\tilde{A}_1, ., \tilde{A}_{12}, ., \tilde{A}_{20}\}$ in position 1 corresponds to $\{\theta_{4BS}, ., \theta_{10BS}, .\theta_{12BS}\}$ whereas $\{\tilde{A}'_1, ., \tilde{A}'_{12}, \ldots, \tilde{A}'_{20}\}$ in position 2 corresponds to $\{\theta_{17BS}, ., \theta_{1BS}, .\theta_{2BS}\}$). Given that the discarded angles eliminates the contribution of different n_o $(\tilde{A}_i)$ values in each ordered set, their impact on $\Delta F_{\hat{Z}}(\hat{z})$ varies. The outcome can be negative if most of the eliminated $\tilde{A}_i$ values were the highest, but this possibility is greatly diminished by identifying the best BS angles in the service area.

A special case is the scenario in which there are two sets of well-separated positions of the user and where the best angles of one group become the worst angles of the other group. Under such conditions, the (n_o) discarded BS angles are mostly linked to the intermediate $\tilde{A}_i$ values at each position. Row 3 in Table 1 shows that even for this scenario, there could be a large percentage of combinations for which $\Delta F_{\hat{Z}}(\hat{z}) \geq 0$.

The elimination of 35% ($n_o = 7$) of BS angles can be realistic in NLOS environments. A severe street canyon propagation may exclude a greater number of angles.

The identification of the best BS angles can be approximated off-line using RT as will be explained in the following section.

B. SIMULATION METHODOLOGY

An accurate 3D commercial RT tool [20] was applied to simulate the wireless channel established between a fixed transmitter BS and UE receivers positioned randomly in a well-defined grid of geographical points or along specific routes that were all under NLOS conditions. The UE received power was predicted for different combinations of BS-UE

antenna directions. The BS power was set to 30 dBm, and the center frequency was set to 28 GHz. A reference[3] (threshold) power level of −85 dBm was considered assuming a signal bandwidth ΔW of 1 GHz, a thermal noise power spectral density of −174 dBm/Hz, a noise figure (NF) of 7 dB and an RF coverage for a minimum rate R of 100 Mbps [12], [21]. The BS and UE used either a combination of ideal sector and isotropic antennas or pyramidal horn antennas of 24.5 dB gain and 10° beamwidth [22], all with vertical polarization. The BS antenna height was set up at 8 m, whereas the UE antenna height was fixed at 1.5 m. Both the BS and UE have only one RF chain. The BS changed the orientation of its horn antenna in different angle ranges depending on the scenario. A 5° angle step in the range [0°, 355°] for the UE antenna orientation was chosen as a compromise between resolution and computation time. The horn antenna can be replaced with a uniform linear/rectangular antenna array (ULA/URA) [23] for the beam switching. The general settings for the tool (Full 3D) were 6 reflections, 1 diffraction and a 0.1° ray spacing.

The study area corresponded to a small city section in Rosslyn, Virginia, USA (Fig. 5) which had a rather intermediate configuration (not a high concentration of buildings or uniformly distributed) and provided opportunity to get data under different street canyon propagation conditions. The exterior buildings walls were assumed to be made of brick. The simulations were divided into two parts: identification of the best BS angles and evaluation of their performance.

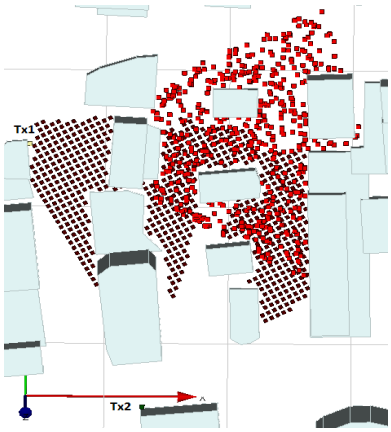

FIGURE 5. Setups 3 and 4 (Tx1/Tx2 center left/bottom).

The simulations were accomplished in two different service areas for comparison. The difference between the setups in the service areas resided in the BS(Tx)-UE(Rx) geographical positions. Tx1 in setup 1 (left center in Fig. 5) was positioned in front of three buildings with heights of 14, 38 and 6 m located across the street at a distance of approximately 48 m, whereas Tx2 in setup 2 (bottom center in Fig. 5) was located in front of a building with a height of 80 m. The positions of the UE considered along the streets were behind the buildings, and thus, NLOS propagation conditions existed. A system assessment using those individual setups is equivalent to an evaluation of two separate sites.

[3]The reference value $P_{ref} = (SNR)(P_n)$ was calculated applying $P_n = -174 + 10log(\Delta W) + NF$ and the relation $R = \beta \Delta W \log_2(1+SNR)$ found in [12], where $\beta = (0.5)\,(0.8)$ for half-TDD constraints and 20% control overhead.

III. APPROXIMATE ANGLE RANGE IDENTIFICATION

The best BS-UE angles were identified by assuming static and slow movers (i.e., nomadic users or pedestrians traveling at speeds below 1.54 km/h), which enables the simplification that all of the UE power measurements for different BS-UE angle combinations can be made at the same UE position or within a distance of 10 λ, where the UE experiences only slight fading [5]. Instead of determining all of the multipath components in the BS-UE link, we focused only on the first propagation path associated with the largest received power; thus, the number of possible beam orientations best illuminating all UE positions was greatly reduced. This strategy was considered reasonable because the field data showed that an average of 2.5 power lobes existed in urban environments [5], and our RT simulations in two specific NLOS service areas indicated an approximate power difference of 10 dB between the first and second propagation lobes, such that the first clearly became the most important one. Considering the use of a threshold level instead of the maximum power value as a decision factor to find the first significant path may rule out some of best BS angles that uniquely serve locations with a maximum power level lower than that threshold. Failure to include those BS angles would have a negative impact on performance.

An RT procedure that can be applied to find the set of best angles consists of predicting the link propagation characteristics for each possible UE position and for all angle combinations of the BS-UE directional antennas. The angles take azimuth and elevation values within certain ranges using small steps. The best BS-UE angle combination corresponds to the maximum power received (P_{rUE_i}) at the UE:

$$\left[\theta^b_{BS}, \emptyset^b_{BS}, \theta^b_{UE}, \emptyset^b_{UE}\right] = \underset{\substack{\theta_{BSmin} \le \theta_{jBS} \theta_{BSmax} \\ \emptyset_{BSmin} \le \emptyset_{kBS} \emptyset_{BSmax} \\ 0 \le \theta_{lUE} < 2\pi \\ \emptyset_{UEmin} \le \emptyset_{qUE} \emptyset_{UEmax} \\ \Delta\theta_{BS}, \Delta\emptyset_{BS}, \Delta\theta_{UE}, \Delta\emptyset_{UE} \\ i=1,2,\ldots,M.}}{\text{argmax}} \left(P_{rUE_i}\right) \quad (5)$$

This procedure becomes impractical due to the long computing time required. Instead, an alternative method suitable for BS antennas installed at low heights (multipath components with small vertical angle variation) is proposed as the following two-step process:

1. *Predict the propagation characteristics for a large number of NLOS points in the area of interest using a sector antenna (e.g., an ideal directional antenna 120° × 20° or 150° × 20°) for the BS and an isotropic antenna for the UE. The UE positions can be chosen to*

form parts of sets of linear routes that are conveniently located or a 2D grid that covers the NLOS service area.

2. *For each UE position, scan the propagation data results by applying a narrow beamwidth antenna in small-angle steps. The total power per scanned angle is calculated as the sum of the individual multipath component powers 'seen' by the scanning antenna. The BS and UE antenna orientation angles where the maximum UE received power occurs (first path) correspond to the angles sought.*

Although the UE received power is diminished in the first step due to the combination of both particular antenna gains, the application of these types of antennas greatly reduces the computation time and renders similar results in the identification of the optimal angles compared to a RT outcome using highly directional antennas. The use of a large number of UE positions in the form of linear routes and 2D grids, which are easy to implement in a modern RT tool [20], helps identify the largest number of best BS-UE angle directions. Moreover, because it is not unusual to find that the same BS angle can be used for the highest RF coverage in many different UE positions, particularly for canyon propagation in urban environments, a non-uniform percentage of RF illumination per BS-UE discrete angle is expected in the application of the proposed method.

The best angles were identified using a 150° directional antenna for the BS (Tx) and an isotropic antenna for the UE in two different service areas. For setup 1 (service area 1), each UE position was part of 21 linear routes (19 parallel to the X,Y axes and 2 sloped). For the majority of points, a separation of 0.1 m along the routes was chosen to record the BS angle variation for very close positions. The distance between some of the routes was set to approximately 5 m. For setup 2, each UE position (1 m separation) belonged to one of three 2D-grids, whose union covered all of NLOS service area 2. Table 2 details the applied linear routes and grids of points.

TABLE 2. Linear routes and grid of points used in the identification of the best BS and UE angles.

Setup 1 BSTx 150° DirectAnt. UERx Isotr. Ant. Data scanTx: set [-60°:1°:60°] Data scanRx: set [0°:1°:359°]	Setup 2 BSTx 150° DirectAnt. UERx Isotr. Ant. Data scan: set [30°:1°:150°] Data scanRx: set [0°:1°:359°]
21 Linear Routes	Total Grid = Union of three smaller grids
12 routes (0.1m): 251 pts each 7 routes (0.1m): 1201, 1202, 1009, 659, 903, 501, 325) = 8,812 pts 1 route (0.75m): 1,532 pts 1 route (0.5m): 121pts Total 10,465 pts	Grid 1 (1m): 3,808pts Grid 2 (1m): 3,987pts Grid 3 (1m): 3,559pts Total 11,354pts

RT output data from the setups in both areas were scanned using a 32-ULA (1° angle step), leveraging the fact that its 3.2° 3 dB-beamwidth [23] facilitated the indication of the BS-UE angle combination for the first path.

The angles and the percentage of UE positions where the application of each BS angle delivers the maximum power are shown in red in Figs. 6 and 7. Set $\mathcal{A}$={−57° to −46°, −43° to −28°, −25°, −18°, 11°, 20° to 30°, 35°, 55° to 60°}, and set $\mathcal{F}$={30° to 36°, 40° to 56°, 58° to 64°, 67° to 75°, 85° to 89°, 103°, 104°, 115° to 143°}, with card($\mathcal{A}$)=49 and card($\mathcal{F}$)=76, were identified for setups 1 and 2, respectively. Fig. 6 shows that the angle ranges ([−16°, 10°], [13°, 18°],….,[37°, 53°]) and other smaller segments were never used. BS angles of −55°, −28° and 25° were the most used.

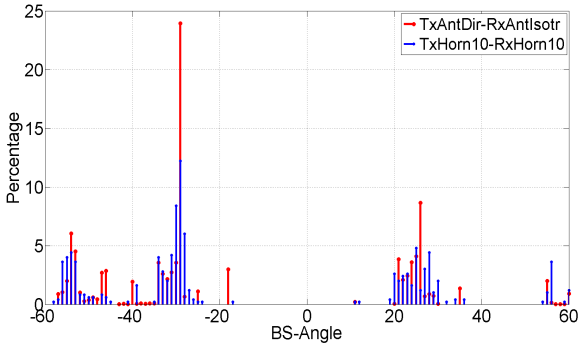

FIGURE 6. Percentage of UEs per BS angle reaching max. power (setups 1 and 3).

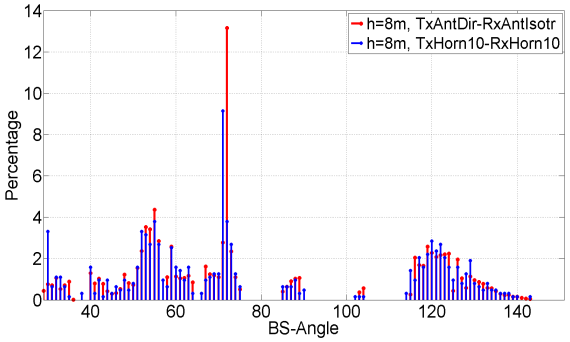

FIGURE 7. Percentage of UEs per BS angle reaching max. power (setups 2 and 4).

In contrast, Fig. 7 shows a smaller number of angle voids and a relatively larger BS angle distribution that was related to a lower building blockage 'seen' by Tx2 in service area 2 than the case of Fig. 6. Fig. 8 shows the percentage of UE positions that reached the maximum possible power per UE angle for both setups. Because these percentages are not equal, we generated four cumulative distribution functions (*cdf*) F_{BS49}, F_{BS76}, F_{UEsc1}, and F_{UEsc2} for subsequent use, assuming that the percentage of UE positions was equivalent to the probability that each angle generated a maximum power. The first two *cdfs* corresponded to the 49 and 76 BS angles, whereas the last two corresponded to the UE angles. The distributions were clearly not uniform.

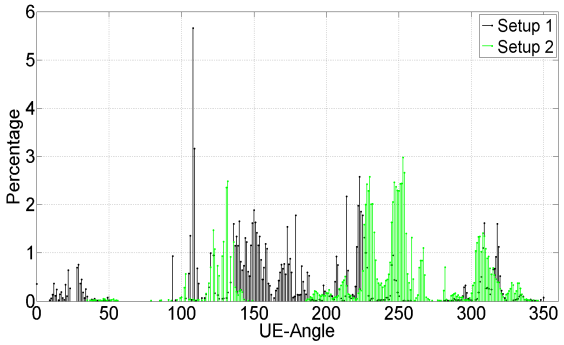

FIGURE 8. Percentage of UE positions per UE angle (max. received power).

To evaluate the proposed method, we contrast its results against an RT outcome from a different setup in each service area, in which the BS and UE were equipped with 10° (3-dB beamwidth) horn antennas.

Setup 3 in service area 1 consists of a BS (Tx1-center left) that illuminates 500 arbitrary positions (red in Fig. 5), whereas setup 4 in service area 2 consists of a BS (Tx2-center bottom) servicing 634 locations uniformly separated by 4 m (black in Fig. 5). A UE located at any of those positions was serviced under the NLOS condition. Sets $\mathcal{C}$ ([−60°:1°: 60°]) and $\mathcal{G}$ ([30°:1°:150°]), with 121 angles each, were used to illuminate the service areas 1 and 2, respectively. Set $\mathcal{Q}$ ([0°:5°:355°]) with 72 angles was applied for the UE antenna beam switching. The best BS-UE angle association was obtained by comparing the received power at the UE for all combinations of the BS and UE angles. A total of 50 (set $\mathcal{B}$={−58° to −49°, −47° to −45°, −41°, −39°, −35° to −24°, −17°, 11°, 12°, 19° to 30°, 32°, 34°, 36°, 54° to 56°, 59° to 60°}) for setup 3 and 79 (set $\mathcal{E}$ = {30° to 35°, 38°, 40° to 64°, 66° to 75°, 85° to 90°, 102° to 104°, 114° to 140°, 143°}) for setup 4 were identified as the best BS angles. Figs. 6 and 7 indicate (blue) the percentages of positions that reached the maximum received power per BS angle in these two setups. An angle identification assessment indicated differences with a small impact on performance. For service area 1, set $\mathcal{A}$ included 11 angles that did not belong to set $\mathcal{B}$, and it did not contain 12 angles that appeared in set $\mathcal{B}$. Those dissimilarities occurred in 7.01% and 4.2% of the UE positions in setups 1 and 3, respectively. For service area 2, set $\mathcal{F}$ showed 3 angles that did not belong in set $\mathcal{E}$, and it did not include 6 angles that appeared in set $\mathcal{E}$. For that area, the differences appeared in 0.17% and 2.52% of the UE positions in setups 2 and 4, respectively.

The maximum power received by the UE in 50 random switches (20,000 iterations) of the BS-UE antenna beam directions allowed the power error to be measured by applying sets $\mathcal{A}(\mathcal{F})$ versus set $\mathcal{B}(\mathcal{E})$. The largest power error found was less than 0.70 dB (0.5 dB in the 50$^{\text{th}}$ percentile) in the case of $\mathcal{A}$ versus $\mathcal{B}$ and less than 0.40 dB (0.2 dB in the 50$^{\text{th}}$ percentile) for $\mathcal{F}$ versus $\mathcal{E}$. Such small differences were anticipated because the angles occupy approximately the same range span, as shown in Figs. 6 and 7.

Increasing the number of linear routes (i.e., decreasing the route separation) in setup 1 improved the accuracy. There was no need to use very close points. In fact, the application of a grid of receivers was better able to uniformly cover the study area. Our simulations in service area 1 that used a grid of 6,004 points separated by 1.5 m yielded similar results. In general, we expected that the UE positions were affected by angle errors less than 5% and by received power errors less than 0.70 dB.

The observed results indicate that the proposed method may constitute a first approximation for the prior identification of the best discrete BS angles that can be applied to improve a directional search procedure.

A closer look at the RF coverage achieved with different subsets of BS angles in setup 3 shows a clear differentiation of their efficacies. Fig. 9 shows the simulation results for the maximum UE power delivery applying four different sets of chosen BS angles. For the case of the BS antenna beam orientations [−55°:10°:55°] (red), the angles of −5°, 5° and 45° statistically provided the worst possibilities for the UE to 'hear' the BS signal compared to other angles, such as −35° and −25°. Although BS angles of −55°, −25° and 25° rendered the best RF illumination in 18.4%, 27.4%, and 28% of the total UE positions, respectively, the angles of −5°, 5° and 45° did not allow for that possibility.

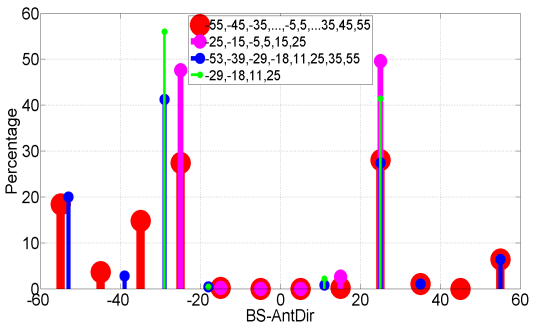

FIGURE 9. Percentage of UE positions per BS angle (max. SNR) in setup 3.

Zero percentage in the maximum power delivery simply means that the remaining angles allowed the BS to provide higher power levels at a UE position relative to that using angles of −5°, 5°, and 45° at the same position. Likewise, the value of 1% obtained with a BS angle of 35° represents the percentage of UE positions with maximum power levels that could not be reached using any other angle in the set [−55°:10°:55°]. The angles of −25° and 25° approximately corresponded to the directions of the streets adjacent to the buildings located in front of Tx1 (Fig. 5), indicating that the positions of the UE considered receive power in the form of street canyon propagation.

Fig. 10 (red lines) shows the percentages of UE positions that did not reach a power value higher than a reference (threshold) level for each specific BS angle. These values are

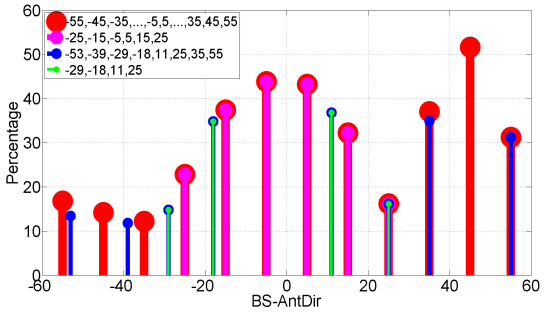

FIGURE 10. Percentage of UE positions per BS angle where power < threshold.

highest for −5°, 5° and 45°. The RF coverage of the different BS angles makes it difficult to be certain that a UE can 'hear' the BS for any specific angle, even if the BS-UE antenna main beams are oriented in the correct direction.

Figs. 9 and 10 also show that although the UE positions were restricted to an area of ±30° × 200 m, some of the best BS angles were outside that scan range. Percentages of 18.4% and 6.4% correspond to angles of −55° and 55°, respectively, that is, in the directions of a neighbor sector within the same cell. If the BS beam orientations were restricted to ±30° (magenta), the percentages for which a maximum UE power delivery occurred increased notably in the directions ±25° (from 28.0(27.4)% to 49.6(47.6)%, respectively), with a negative impact on the total number of UEs that could not achieve a power level above the threshold because that value increased from 1.6% (8 UE) to 5.4% (27 UEs). Nevertheless, even for this last scenario, −5° and 5° remained the most inefficient angles for RF coverage.

As anticipated, although many UE positions may not reach some minimum power level for a particular BS beam direction, the same position can be covered by the base station using a different angle. Fig. 11 shows the statistics obtained in setup 3 using five different groups of angles. The statistics remained fairly constant when the number of equally spaced angles was reduced from 12 (red) to 9 (yellow curve), that is, not using angles of −5°, 5°, and 45° because they did not contribute to the highest power levels.

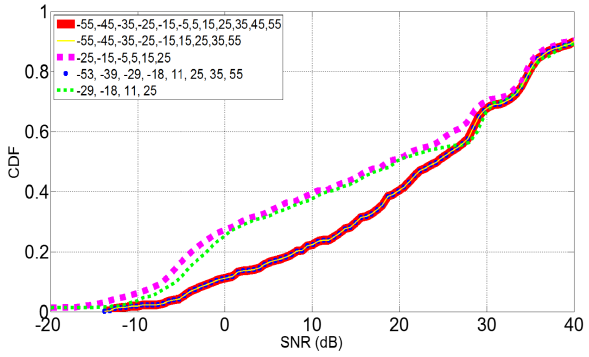

FIGURE 11. SNR at UE positions (500).

Fig. 11 also shows that there was no significant difference in performance between the sets of the equally spaced (red) and chosen (blue) angles, although there were 4 fewer angles (12 versus 8). For this latter figure, some of the maximum power values obtained for BS discrete angles restricted in the range ±30° took lower levels than what could be obtained using others outside that range.

IV. PERFORMANCE IMPACT

To quantify the performance benefit of using a reduced set of the best BS angles (49 and 76 for service areas 1 and 2, respectively), we applied such a set in a system that changed the BS and UE angles randomly L times over a period T to determine the best link angles $(\theta_{BS}, \theta_{UE})$. We considered the following cases:

A. MAXIMUM RECEIVED SNR USING THE COMPLETE AND BEST SETS OF BS ANGLES

Comparisons of the maximum SNRs received using the identified best BS angles with respect to the complete group of 121 angles in setups 3 and 4 are shown in Figs. 12 and 13, respectively. In both figures, 'the maximum possible SNR' is plotted in green. These last curves represent the highest SNR value obtained after examining all possible combinations of the 121 discrete BS and 72 UE angles.

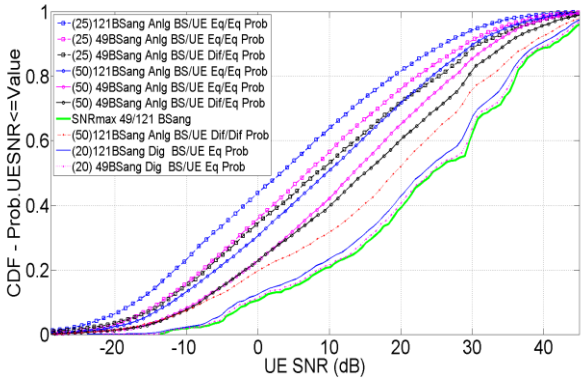

FIGURE 12. UE maxSNR in 50 (25) measurements – 121 vs. 49 BS angles (setup 3).

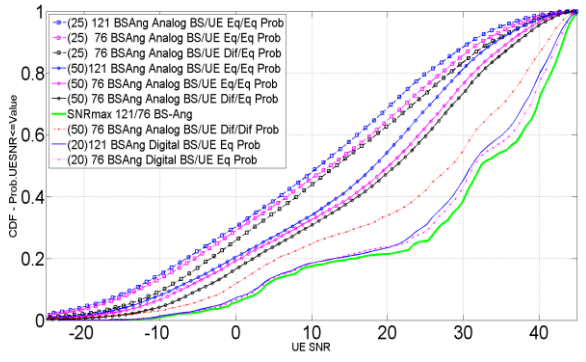

FIGURE 13. UE maxSNR in 50 (25) measurements – 121 vs. 76 BS angles (setup 4).

Fig. 12 shows two groups ($L = 25, 50$) of three plots (blue/magenta/black) representing the maximum received SNR under the following conditions: a) the BS angles from set $\mathcal{C}$ (121) applied with equal probability values; b) the BS angles from set $\mathcal{A}$ (best 49) used with equal probabilities and c) the BS angles from set $\mathcal{A}$ applied with different probability values according to the distribution function F_{BS49}. In all three cases, the UE changed the angles from the set $\mathcal{Q}$ (=[0°:5°:355°]), with equal probabilities. The simulations indicated that the SNR obtained for case b was on average 3.03 dB (50th percentile, L =50) larger than that obtained for case a because the 49 angles contributed the 'highest' levels of power at the UE positions and were generated with a larger probability (1/49 versus 1/121). In other words, assigning a zero probability to the 72 (=121-49) BS angles in the set '$\mathcal{C}$ - $\mathcal{A}$' and increased equal probabilities to the remainder led to improved performance. Furthermore, assigning different probabilities to the elements of set $\mathcal{A}$ based on the *cdf* F_{BS49} rendered an additional benefit of 2.1 dB (50th percentile, $L = 50$), yielding an overall average gain of 5.13 dB. The latter performance gain began from a SNR≥3 dB.

Fig. 12 also shows (red dash-dot line) that a potential increase of 4 dB (50th percentile) may be possible in the hypothetical circumstance in which the UE, assuming that it has the same spatial reference of the BS, varies its antenna beam direction randomly according to a *cdf* F_{UEsc1} passed by the BS and previously obtained off-line from RT data.

Fig. 12 includes the ideal case of a UE capable of estimating the main AoA of the first path for each BS angle (solid blue/dash-dot magenta curves) and reporting the maximum power received after L trials (i.e., digital beamforming). We used only $L = 20$ because the plots basically coincide with 'the maximum possible SNR' curves for larger values of L, revealing a small opportunity for improvement. Nevertheless, even for this ideal case, there is a potential gain when L decreases. As expected, the figure also indicates (green curve) that the maximum power obtained by applying set $\mathcal{A}$ (best 49) was the same as for set $\mathcal{C}$ (full 121 angles) and that a reduced number of UE readings ($L = 25$) per period resulted in a lower received power.

Fig. 13 shows the same plots presented in Fig. 12 but for setup 4. The overall SNR gain, including the BS angle variation based on *cdf* F_{BS76}, reached 2.65 (1.85+0.8) dB in the 50th percentile ($L = 50$), which was lower than that obtained from setup 3. This result suggests that the performance improvement gain was related to the canyon propagation severity, which was higher in service area 1 (Fig. 5). Similarly, if the UE had the same spatial reference as the BS, the use of random beam orientations generated from F_{UEsc2} would represent an additional gain of approximately 7 dB, which becomes interesting in terms of potential performance improvements based on knowledge of the propagation characteristics. A smaller number of best BS angles for RF illumination led to a higher performance gain because their more frequent application (49 for service area 1 versus 76 for service area 2) in a defined time period generated larger average power levels at the UE positions

An evaluation of $\Delta F_{\hat{Z}}(\hat{z}) = F_{\hat{Z}_1}(\hat{z}) - F_{\hat{Z}_2}(\hat{z})$ using (2) and (4) for all positions of the user in the two service areas provides an alternative vision of the RT results. Each position has a different set of $\tilde{A}_i$ values ($i = 1, 2, .., 121$) linked to a different distribution of the 121 angles (e.g., position 1 has $\left\{\tilde{A}_1, \tilde{A}_2, \ldots, \tilde{A}_{121}\right\}$ associated with $\{\theta_{1BS}, \theta_{2BS}, .., \theta_{121BS}\}$, whereas position 2 has $\left\{\tilde{A}'_1, \tilde{A}'_2, ., \tilde{A}'_{121}\right\}$ related to $\{\theta_{5BS}, .\theta_{121BS}, .\theta_{10BS}\}$).

The application of the reduced set of best angles means discarding different $\tilde{A}_i$ values in different locations. In general we applied the parameters $\theta^{\Delta}_{3dB} = 10°$, $\theta^{\Delta}_{a} = 5°$, $\theta^{\Delta}_{b} = 15°$, $L = 50$ and $N = 121$. Specifically $F_{\hat{Z}_2}(\hat{z})$ was calculated with the probability values of 1/49 and 1/76 in service areas 1 and 2, respectively, whereas $F_{\hat{Z}_1}(\hat{z})$ used the value of 1/121 for all 121 $\tilde{A}_i$ values in both service areas. For each UE position, we calculated 10,001 values of $\Delta F_{\hat{Z}}(\hat{z})$ due to the large difference between the minimum and maximum $\tilde{A}_i$ values (>40dB).

The percentage of user positions at which $\Delta F_{\hat{Z}}(\hat{z}) \geq 0$ provides an estimate of the efficacy of the proposed method to improve the performance. Assuming that a positive result means that at least 99.5% of the 10,001 values of $\Delta F_{\hat{Z}}(\hat{z})$ are greater than or equal to zero at any location, then Table 3 indicates that the proposed method provides an opportunity for improvement in 82.8% and 64.7% of the UE positions in service areas 1 and 2, respectively. Clearly, the improvement is greater in service area 1 where there are a smaller number of best BS angles.

TABLE 3. Percentage of positions of the user where $\Delta F_{\hat{Z}}(\hat{z}) \geq 0$ in the service areas 1 and 2.

	$\Delta F_{\hat{Z}}(\hat{z}) \geq 0$ (all 10,001 values) or $\Delta F_{\hat{Z}}(\hat{z}) < 0$ in less than (X)% of the 10,001 values				
	X=0.0	X=0.25	X=0.5	X=1.0	X=2.0
500 UEs 49 BS angles	66.4%	81.0%	82.8%	83.0%	91.0%
634 UEs 76 BS angles	28.4%	57.3%	64.7%	70.2%	75.1%

B. MAXIMUM RECEIVED SNR USING A LIMITED NUMBER OF BS ANGLES

A performance comparison of a group of equally spaced angles with larger separation relative to the same number of chosen directions showed a higher gain. For this task, we contrasted 25 BS angles from the sets ([−60°:5°:60°], [30°:5°:150°])) to angles chosen from the previously identified sets $\mathcal{A}$ and $\mathcal{F}$. Two different approaches were followed.

i) In descending order, we sorted the percentage of UE positions per BS angle obtained from the application of the proposed method in setups 1 and 2 and selected the 25 angles with the largest percentages.

ii) We applied the following search objective to the data obtained from the simulations in setups 3 and 4:

$$e_T = min\left[\sum_{i=1}^{M} |p_{iN} - p_{ik}|_{\,all\binom{N}{k}\ of\ BS\ angles}\right], \quad (6)$$

where

$$p_{iN} = \max\left(P_{i,1}, P_{i,2}, P_{i,3}, \ldots\ldots, P_{i,N}\right),$$
$$p_{ik} = \max(P_{i,n_1}, P_{i,n_2}, \ldots\ldots\ldots, P_{i,n_k});\ \ n_1, \ldots., n_k \leqslant N$$

and

$$(\theta_{n_1 BS}, \theta_{n_2 BS}, .., \theta_{n_k BS}) \in \left\{\binom{N}{k} \text{ of } [\theta_{1BS}, \theta_{2BS}, .., \theta_{NBS}]\right\}.$$

$P_{i,j}$ represents the partial maximum power at a UE with position i (UEi) considering all of the power values measured when the UE antenna beam is rotated 360° in 5° steps for a particular BS angle θ_{jBS}. p_{iN} and p_{ik} correspond to the 'maximum possible power' at UEi considering all N and k BS-angles, respectively. e_T must be evaluated for all k-combinations of N BS angles and for all M positions.

Because $C(N,k) = \binom{N}{k}$ generates a large number of combinations (e.g., $C(76,25) \approx 7.8367 \times 10^{19}$), it is difficult to evaluate the objective function using an exhaustive search. Instead, we used a binary genetic algorithm (with k-gene chromosomes) to approximate the best combination of BS angles [24].

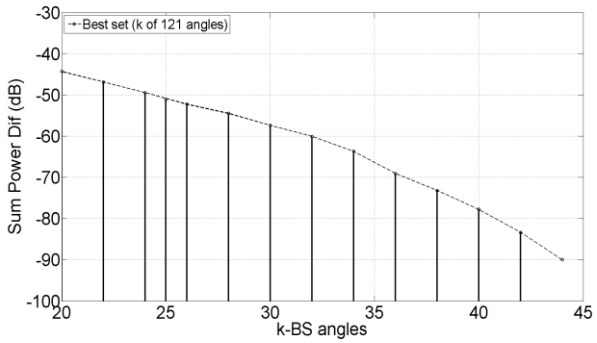

FIGURE 14. Sum of power diff. (dB) vs. k-BS angle groups (setup 3).

Fig. 14 shows that the sum of the power differences (6) decreased as the best set of k-BS angles increased. For $k > 42$, this value becomes extremely small, indicating that a large fraction of the 121 angles in setup 3 did not contribute to a maximum power.

Fig. 15 shows the simulation of the maximum SNR at the UE in $L = 50$ measurements, assuming an equal probability for the BS and UE angle switching (10,000 iterations). The angles selected when applying approach ii) demonstrated better performances (solid black and blue lines) of approximately 4.40 dB and 2.80 dB on average compared to the 25 equally spaced angles (black and blue dotted lines) for setups 3 and 4, respectively. These results reiterated the lower

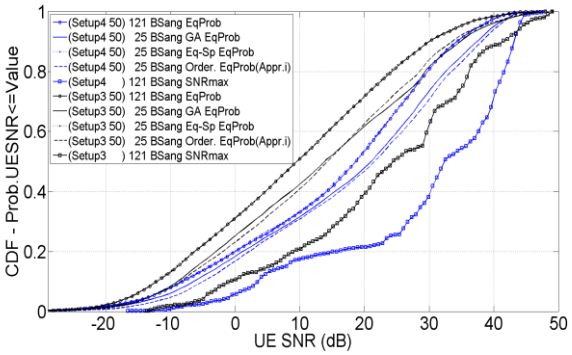

FIGURE 15. 25 BS equally spaced versus 25 selected angles in setup 3 and 4.

gain for service area 2. The application of the first approach (i) (black and blue dashed lines) is computationally simpler and produces results within 1.7 dB compared to those obtained with approach (ii).

C. NUMBER OF SWITCHES IN A BEAM-TRAINING PROCEDURE

A particular initial beam-training procedure in which the BS repeats the same BS angle for a number of UE beam shifts benefits from the knowledge of the most effective BS angles.

Our simulation in setup 3 (Fig. 16) shows that the number of sequential beam shifts (5°) needed until the UE received a power level equal or larger than a reference threshold decreased when a selected set of BS angles was used. It was assumed that the UE had an initial arbitrary beam direction.

Specifically, the comparison of the full set of 121 BS angles versus the 49 BS (best) angles indicates that the number of UE beam switches decreased from 46 to 32 (50^{th} percentile) when the BS changed the beam directions, whether sequentially or randomly (uniform distribution). Three additional beam shifts were saved if the 49 BS angles changed values according to the coverage distribution function F_{BS49} (red line). The percentage (per BS angle) of trials in which the link connection could not be established in 72 beam switches (360°) decreased from 38% to 27%.

Fig. 16 also shows that the performance of the 25 equally spaced BS angles was approximately the same as that of the full set of 121 angles.

D. MAXIMUM RECEIVED SNR FOR A MOBILE USER USING A LIMITED NUMBER OF BS ANGLES

Fig. 17 shows a comparison of the 25 best BS antenna orientations chosen from set $\mathcal{A}$ versus 25 equally spaced angles ([−60°:5°:60°]) for the case of a UE moving at 30 km/h in setup 3. The BS and UE switched their beams randomly with equal probability. Ten linear routes, each of 50 points separated by 4.1667 cm (total distance=2.08 m), were applied such that the UE measured the received power at a displaced position at each new BS angle switch time ($L = 50$). The selected routes were placed to be well separated and were oriented in different directions inside service area 1.

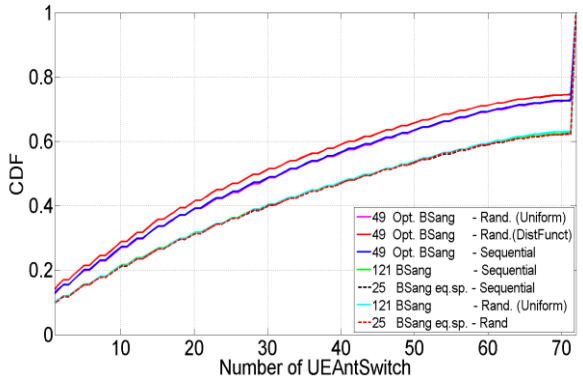

FIGURE 16. sequential beam switches until power ≥ threshold in setup 3.

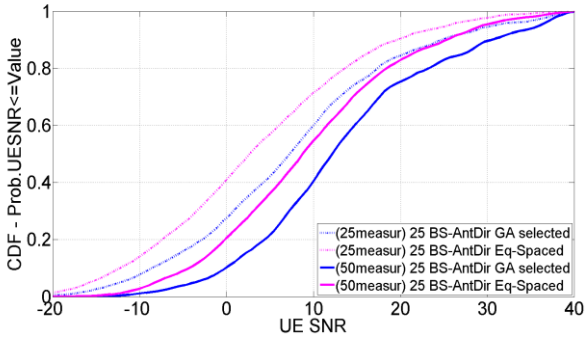

FIGURE 17. SNR statistics for a mobile user (30 km/h) in setup 3.

In this scenario, a performance gain of 3.3 dB (50th percentile) was obtained. This lower gain (than the static case) appears to be compatible with the method of determining the maximum power in 50 different positions along each route and averaging over many iterations. The power sample values depended on the spatial power distribution generated using each discrete BS angle, the UE beam orientations, and the speed and direction of the user.

V. CONCLUSIONS

The results from RT simulations in the 28 GHz band suggest that *a priori* information regarding the efficacy of some discrete BS angles to deliver the maximum power possible at NLOS locations within a service area can be exploited in a directional cell search or in the initial part of a beam training procedure, particularly for cases in which the BS and UE apply analog beamforming. A performance gain of more than 2 dB was obtained when both the BS and UE changed their beam orientations randomly, but this result may depend on the severity of the street canyon propagation and the probability of angle use. The percentage of UE positions per BS angle in which the maximum received power is reached may also be applied to improve the performance further. The approximate identification of the best BS angles can be accomplished using a simple RT procedure.

APPENDIX A

Assumptions:

a) User located at position x from the BS.

b) For each discrete BS angle θ_{iBS}, there is only one multipath component with amplitude $\tilde{A}_i$ arriving at the UE in the direction $\theta_{UEalign}$. N angles θ_{iBS} and $\tilde{A}_1 < \tilde{A}_2 < \tilde{A}_3 < \ldots < \tilde{A}_N$ were assumed.

c) The gain of the UE antenna $Y = g_u(\theta^\Delta)$ has the form shown in Fig. 3 (1), where $\theta^\Delta = (\theta_{UEalig} - \theta_{UE})$ - is the difference in UE azimuth angles between the antenna main direction aligned with the arriving multipath component and an arbitrary UE antenna orientation. θ^Δ takes values according to a uniform distribution, that is, $\theta^\Delta \sim U(-\pi, \pi]$.

A. DISTRIBUTION AND DENSITY FUNCTION OF THE UE ANTENNA GAIN - $g_u(\theta^\Delta)$

The cumulative distribution function (*cdf*) $F_Y(y) = P\left\{g_u(\theta^\Delta) \le y\right\}$ can be calculated [19] as

$$y < 0 \quad F_Y(y) = 0, \tag{7a}$$

$$y \ge 1 \quad F_Y(y) = 1, \tag{7b}$$

$$0 \le y < 1,$$

$$F_Y(y) = 2\,\text{Prob}\left\{\theta^\Delta > \frac{y-b}{m}\right\},$$

$$F_Y(y) = 1 + \frac{1}{\pi}\left[2y\left(\theta^\Delta_{3dB} - \theta^\Delta_a\right) - \left(2\theta^\Delta_{3dB} - \theta^\Delta_a\right)\right], \tag{7c}$$

and

$$F_Y(0) = 1 - \frac{1}{\pi}\left(2\theta^\Delta_{3dB} - \theta^\Delta_a\right) = 1 - \frac{\theta^\Delta_b}{\pi}, \tag{7d}$$

where we applied the following relations obtained from Fig. 3:

$$\frac{1/2}{\left(\theta^\Delta_{3dB} - \theta^\Delta_a\right)} = \frac{1}{\theta^\Delta_b - \theta^\Delta_a}, \tag{8}$$

$$y = m\theta^\Delta + b = -\frac{\theta^\Delta}{\theta^\Delta_b - \theta^\Delta_a} + \frac{2\theta^\Delta_{3dB} - \theta^\Delta_a}{2\left(\theta^\Delta_{3dB} - \theta^\Delta_a\right)}, \tag{9}$$

and

$$2\,\text{Prob}\left\{\theta^\Delta > \frac{y-b}{m}\right\} = \frac{2}{2\pi}\left(\pi - \frac{y-b}{m}\right) = 1 - \frac{1}{\pi}\left(\frac{y - \frac{2\theta^\Delta_{3dB} - \theta^\Delta_a}{2\left(\theta^\Delta_{3dB} - \theta^\Delta_a\right)}}{-\frac{1}{\theta^\Delta_b - \theta^\Delta_a}}\right) \tag{10}$$

Taking the first derivative of $F_Y(y)$ (7a, 7b, and 7c) and using (8), the probability density function (*pdf*) of Y (Fig. 18) becomes

$$f_Y(y) = \left(1 - \frac{\theta^\Delta_b}{\pi}\right)\delta(y) + \left(\frac{\theta^\Delta_b - \theta^\Delta_a}{\pi}\right)\text{rect}(y - 1/2) + \frac{\theta^\Delta_a}{\pi}\delta(y-1) \tag{11}$$

where rect(y) and $\delta(y)$ are the rectangular and impulse functions, respectively.

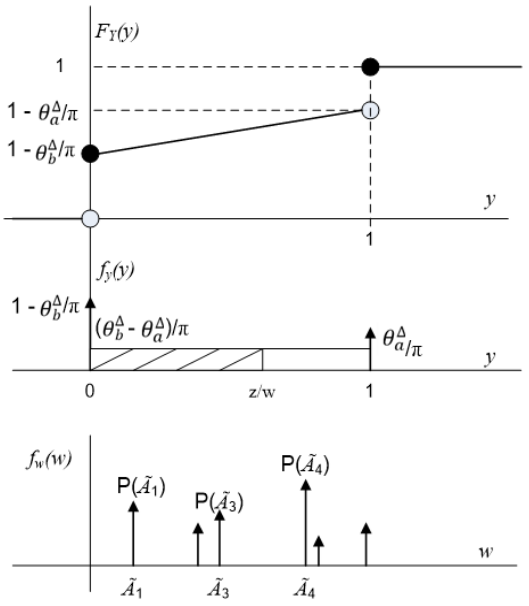

FIGURE 18. *cdf* and *pdf* of $Y = g_u(\theta^\Delta)$ and $f_{W(w)}$. $\tilde{A}_1 < \tilde{A}_2 < \tilde{A}_3 < \ldots < \tilde{A}_N$.

B. DISTRIBUTION FUNCTION OF AN INDIVIDUAL UE POWER READING $F_Z(z)$

Assume the BS uses θ_{iBS} with $p_{\theta_{iBS}}$. Let the maximum possible power level (UE and BS have their antenna beams aligned) at a UE located at $x = x_i$ is a random variable $\tilde{A}$ taking values from the set $\left\{\tilde{A}_1, \tilde{A}_2, \ldots, \tilde{A}_i, .., \tilde{A}_N\right\}$ with $\text{Prob}(\tilde{A}_i) = \text{Prob}(\theta_{iBS})$. Then the *cdf* of the power $Z = \tilde{A} g_u(\theta^\Delta)$ read by the UE for any antenna orientation is computed [19] as

$$F_Z(z) = \int_0^\infty \int_0^{\frac{z}{w}} f_W(w) f_y(y)\, dwdy, \tag{12}$$

where

$$f_W(w) = \sum_{i=1}^{N} p_{\tilde{A}_i} \delta\left(w - \tilde{A}_i\right). \tag{13}$$

$\tilde{A}$ and $g_u(\theta^\Delta)$ are considered independent random variables.

Replacing (13) in (12), we obtain

$$\begin{aligned} F_Z(z) = &\int_0^\infty p_{\tilde{A}_1} \delta\left(w - \tilde{A}_1\right) \int_0^{\frac{z}{w}} f_Y(y)\, dydw \\ &+ \int_0^\infty p_{\tilde{A}_2} \delta\left(w - \tilde{A}_2\right) \int_0^{\frac{z}{w}} f_Y(y) dydw \\ &+ \ldots + \int_0^\infty p_{\tilde{A}_N} \delta\left(w - \tilde{A}_N\right) \int_0^{\frac{z}{w}} f_Y(y) dydw. \end{aligned} \tag{14}$$

The first term exists only for $w = \tilde{A}_1$. A similar condition applies for the remaining terms.

$F_Z(z)$ is explicitly calculated as

$\underline{z < \tilde{A}_1}$

For this case, $f_Y(y)$ in the first term of (14) does not include the impulse $\frac{\theta_a^\Delta}{\pi}\delta(y-1)$ because this term is different from zero only for $w = \tilde{A}_1$ and $z < \tilde{A}_1$, which results in $y = z/w < 1$. The same applies for the remaining terms, given that $\tilde{A}_1 < \tilde{A}_2 < \tilde{A}_3 < \ldots < \tilde{A}_N$.

$$\begin{aligned} F_Z(z) = &\int_0^\infty p_{\tilde{A}_1} \delta\left(w - \tilde{A}_1\right) \\ &\cdot \left[\left(1 - \frac{\theta_b^\Delta}{\pi}\right) + \left(\frac{\theta_b^\Delta - \theta_a^\Delta}{\pi}\right)\frac{z}{w}\right] dw \\ &+ \int_0^\infty p_{\tilde{A}_2} \delta\left(w - \tilde{A}_2\right) \\ &\cdot \left[\left(1 - \frac{\theta_b^\Delta}{\pi}\right) + \left(\frac{\theta_b^\Delta - \theta_a^\Delta}{\pi}\right)\frac{z}{w}\right] dw \\ &+ \ldots + \int_0^\infty p_{\tilde{A}_N} \delta\left(w - \tilde{A}_N\right) \\ &\cdot \left[\left(1 - \frac{\theta_b^\Delta}{\pi}\right) + \left(\frac{\theta_b^\Delta - \theta_a^\Delta}{\pi}\right)\frac{z}{w}\right] dw \\ F_Z(z) = &\left(1 - \frac{\theta_b^\Delta}{\pi}\right) + \left(\frac{\theta_b^\Delta - \theta_a^\Delta}{\pi}\right) z \left[\sum_{i=1}^{N} \frac{p_{\tilde{A}_i}}{\tilde{A}_i}\right] \end{aligned} \tag{15}$$

$\underline{\tilde{A}_1 \le z < \tilde{A}_2}$

$f_Y(y)$ in the first term of (14) must include the second impulse component $\frac{\theta_a^\Delta}{\pi}\delta(y-1)$ because $z/w > 1$. For the remaining terms, $z/w < 1$ and

$$\begin{aligned} F_Z(z) = &p_{\tilde{A}_1} + \int_0^\infty p_{\tilde{A}_2} \delta\left(w - \tilde{A}_2\right) \\ &\cdot \int_0^{\frac{z}{w}} \left[\left(1 - \frac{\theta_b^\Delta}{\pi}\right)\delta(y) + \left(\frac{\theta_b^\Delta - \theta_a^\Delta}{\pi}\right)\right] dydw \\ &+ \ldots + \\ &+ \int_0^\infty p_{\tilde{A}_N} \delta\left(w - \tilde{A}_N\right) \\ &\cdot \int_0^{\frac{z}{w}} \left[\left(1 - \frac{\theta_b^\Delta}{\pi}\right)\delta(y) + \left(\frac{\theta_b^\Delta - \theta_a^\Delta}{\pi}\right)\right] dydw, \\ F_Z(z) = &p_{\tilde{A}_1} + \sum_{i=2}^{N} p_{\tilde{A}_i} \left[\left(1 - \frac{\theta_b^\Delta}{\pi}\right) + \left(\frac{\theta_b^\Delta - \theta_a^\Delta}{\pi}\right)\frac{z}{\tilde{A}_i}\right], \\ F_Z(z) = &\left(1 - \frac{\theta_b^\Delta}{\pi}\right) + \left(\frac{\theta_b^\Delta}{\pi}\right) p_{\tilde{A}_1} \\ &+ \left(\frac{\theta_b^\Delta - \theta_a^\Delta}{\pi}\right) z \left[\sum_{i=2}^{N} \frac{p_{\tilde{A}_i}}{\tilde{A}_i}\right]. \end{aligned} \tag{16}$$

$\underline{\tilde{A}_2 \le z < \tilde{A}_3,}$

$$\begin{aligned} F_Z(z) = &\left(1 - \frac{\theta_b^\Delta}{\pi}\right) + \left(\frac{\theta_b^\Delta}{\pi}\right)\left(p_{\tilde{A}_1} + p_{\tilde{A}_2}\right) \\ &+ \left(\frac{\theta_b^\Delta - \theta_a^\Delta}{\pi}\right) z \left[\sum_{i=3}^{N} \frac{p_{\tilde{A}_i}}{\tilde{A}_i}\right]. \end{aligned} \tag{17}$$

In general, for $\tilde{A}_{j-1} \leq z < \tilde{A}_j$,

$$F_Z(z) = \left(1 - \frac{\theta_b^\Delta}{\pi}\right) + \left(\frac{\theta_b^\Delta}{\pi}\right) \sum_{i=1}^{j-1} p_{\tilde{A}_i} + \left(\frac{\theta_b^\Delta - \theta_a^\Delta}{\pi}\right) z \left[\sum_{i=j}^{N} \frac{p_{\tilde{A}_i}}{\tilde{A}_i}\right]. \quad (18)$$

For $z \geq \tilde{A}_N$, $F_z(z) = 1$ because all terms in (14) include the second impulse $\frac{\theta_a^\Delta}{\pi}\delta(y-1)$.

For simplicity, we include in (18) the case where $j = 1$, in which the first summation $\sum_{i=1}^{j-1} p_{\tilde{A}_i} = 0$ and $\tilde{A}_0 = 0$, although this power level does not exist.

C. DISTRIBUTION FUNCTION OF THE MAXIMUM POWER IN L READINGS – $F_Z(z)$

If Z_i is the power obtained at the UE location in one reading, then the *cdf* of $\hat{Z} = \max[Z_1\ Z_2 \ldots\ldots\ Z_L]$ in L readings corresponds to $F_{\hat{Z}}(\hat{z}) = F_{Z_1}(\hat{z}) F_{Z_2}(\hat{z}) \ldots F_{Z_l}(\hat{z}) \ldots F_{Z_L}(\hat{z})$, where each $F_{Z_l}(\hat{z})$ is given by (18).

ACKNOWLEDGMENTS

The authors thank Professor Sixto Garcia from ESPOL for his advice in the application of genetic algorithms.

REFERENCES

[1] *Cisco Visual Networking Index: Global Mobile Data Traffic Forecast Update, 2015–2020, White Paper*, CISCO, San Jose, CA, USA, 2016.
[2] F. Khan and Z. Pi, "mmWave mobile broadband (MMB): Unleashing the 3–300GHz spectrum," in *Proc. 34th IEEE Sarnoff Symp.*, May 2011, pp. 1–6.
[3] H. Zhao *et al.*, "28 GHz millimeter wave cellular communication measurements for reflection and penetration loss in and around buildings in New York City," in *Proc. IEEE Int. Conf. Commun.*, Budapest, Hungary, Jun. 2013, pp. 5163–5167.
[4] Y. Azar *et al.*, "28 GHz propagation measurements for outdoor cellular communications using steerable beam antennas in New York city," in *Proc. IEEE Int. Conf. Commun.*, Budapest, Hungary, Jun. 2013, pp. 5143–5147.
[5] M. Samimi *et al.*, "28 GHz angle of arrival and angle of departure analysis for outdoor cellular communications using steerable beam antennas in New York City," in *Proc. IEEE 77th Veh. Technol. Conf. Spring*, Dresden, Germany, Jun. 2013, pp. 1–6.
[6] S. Rangan, T. S. Rappaport, and E. Erkip, "Millimeter-wave cellular wireless networks: Potentials and challenges," *Proc. IEEE*, vol. 102, no. 3, pp. 366–385, Mar. 2014.
[7] T. S. Rappaport, E. Ben-Dor, J. N. Murdock, and Y. Qiao, "38 GHz and 60 GHz angle-dependent propagation for cellular & peer-to-peer wireless communications," in *Proc. IEEE Int. Conf. Commun.*, Ottawa, ON, Canada, Jun. 2012, pp. 4568–4573.
[8] T. S. Rappaport, F. Gutierrez, Jr., E. Ben-Dor, J. N. Murdock, Y. Qiao, and J. I. Tamir, "Broadband millimeter-wave propagation measurements and models using adaptive-beam antennas for outdoor urban cellular communications," *IEEE Trans. Antennas Propag.*, vol. 61, no. 4, pp. 1850–1859, Apr. 2013.
[9] M. Giordani, M. Mezzavilla, and M. Zorzi. (Feb. 2016). "Initial access in 5G mm-wave cellular networks." [Online]. Available: http://arxiv.org/abs/1602.07731
[10] V. Desai, L. Krzymien, P. Sartori, W. Xiao, A. Soong, and A. Alkhateeb, "Initial beamforming for mmWave communications," in *Proc. 48th Asilomar Conf. Signals, Syst., Comput.*, Nov. 2014, pp. 1926–1930.
[11] C. Jeong, J. Park, and H. Yu, "Random access in millimeter-wave beamforming cellular networks: Issues and approaches," *IEEE Commun. Mag.*, vol. 53, no. 1, pp. 180–185, Jan. 2015.
[12] C. N. Barati, S. A. Hosseini, S. Rangan, P. Liu, T. Korakis, and S. S. Panwar, "Directional cell search for millimeter wave cellular systems," in *Proc. IEEE 15th Int. Workshop Signal Process. Adv. Wireless Commun.*, Toronto, ON, Canada, Apr. 2014, pp. 120–124.
[13] P. A. Eliasi, S. Rangan, and T. S. Rappaport. (Oct. 2014). "Low-rank spatial channel estimation for millimeter wave cellular systems." [Online]. Available: http://arxiv.org/abs/1410.4831
[14] A. Alkhateeb, O. El Ayach, G. Leus, and R. W. Heath, Jr., "Channel estimation and hybrid precoding for millimeter wave cellular systems," *IEEE J. Sel. Topics Signal Process.*, vol. 8, no. 5, pp. 831–846, Oct. 2014.
[15] M. R. Akdeniz *et al.*, "Millimeter wave channel modeling and cellular capacity evaluation," *IEEE J. Sel. Areas Commun.*, vol. 32, no. 6, pp. 1164–1179, Jun. 2014.
[16] J. Kim and A. F. Molisch, "Fast millimeter-wave beam training with receive Beamforming," *J. Commun. Netw.*, vol. 16, no. 5, pp. 512–522, Oct. 2014.
[17] A. Capone, I. Filippini, and V. Sciancalepore. (Jan. 2015). "Context information for fast cell discovery in mm-wave 5G networks." [Online]. Available: http://arxiv.org/abs/1501.02223
[18] S. Akoum, O. El Ayach, and R. W. Heath, Jr., "Coverage and capacity in mmWave cellular systems," in *Proc. 46th Asilomar Conf. Signals, Syst. Comput.*, Pacific Grove, CA, USA, Nov. 2012, pp. 688–692.
[19] A. Papoulis and S. U. Pillai, *Probability, Random Variables and Stochastic Processes*, 4th ed. New York, NY, USA: McGraw-Hill, 2002, pp. 124–125.
[20] RemCom. (2016). *Wireless InSite*. [Online]. Available: http://www.remcom.com/wireless-insite
[21] M. Abouelseoud and G. Charlton, "System level performance of millimeter-wave access link for outdoor coverage," in *Proc. IEEE Wireless Commun. Netw. Conf.*, Shanghai, China, Apr. 2013, pp. 4146–4151.
[22] C. A. Balanis, *Antenna Theory: Analysis and Design*, 3rd ed. Hoboken, NJ, USA: Wiley, 2005, pp. 769–783.
[23] H. L. Van Trees, *Optimum Array Processing: Part IV of Detection, Estimation, and Modulation Theory*. Hoboken, NJ, USA: Wiley, 2002, ch. 2, p. 48.
[24] R. E. Haupt and S. L. Haupt, *Practical Genetic Algorithms*, 2nd ed. Hoboken, NJ, USA: Wiley, 2004, ch. 2, pp. 27–47.

JUAN C. AVILES (M'10) received the degree in electrical engineer from Escuela Superior Politecnica del Litoral (ESPOL) in 1982, and the M.S. degree in electrical engineering from Syracuse University in 1986. He is currently pursuing the Ph.D. degree with the École de technologie supérieure, Montréal, Canada. He has been a Professor with the Faculty of Electrical and Computer Engineering, ESPOL and an Advisor in the radio communications field. His research interests are propagation and intelligent antenna applications for mobile systems in mmW bands.

AMMAR KOUKI (S'88–M'92–SM'01) received the B.S. (Hons.) and M.S. degrees in engineering science from Pennsylvania State University, in 1985 and 1987, respectively, and the Ph.D. degree in electrical engineering from the University of Illinois at Urbana–Champaign in 1991. He is currently a Full Professor of Electrical Engineering and the Founding Director of the LTCC@ETS Laboratory with École de technologie supérieure, Montréal, Canada. His research interests are in the areas of active and passive microwave and mm-wave devices and circuits, intelligent and efficient RF front-ends, 3-D circuits in LTCC, applied computational electromagnetics and antennas radio-wave propagation modeling.